Fermi surface gapping in the Dirac material Ca_{1−x}Na_{x}MnBi_{2}

M. Corasaniti, R. Yang, A. Pal, M. Chinotti, L. Degiorgi, A. Wang, and C. Petrovic

Phys. Rev. B **100**, 041107 — Published 12 July 2019

DOI: 10.1103/PhysRevB.100.041107

Proneness towards Fermi surface gapping in the Dirac material $Ca_{1-x}Na_xMnBi_2$

M. Corasaniti[+], R. Yang[+], A. Pal, M. Chinotti, and L. Degiorgi[*]
Laboratorium für Festkörperphysik, ETH - Zürich, 8093 Zürich, Switzerland

A. Wang[†] and C. Petrovic
Condensed Matter Physics and Materials Science Department, Brookhaven National Laboratory, Upton NY 11973, USA

(Dated: June 26, 2019)

The newly designed AMnBi$_2$ (A = alkaline as well as rare earth atom) materials based on quasi-two-dimensional bismuth layers provide a suitable playground to address the physics of Dirac fermions, in connection with magnetism and structural changes. Here, we perform an optical investigation as a function of temperature of $Ca_{1-x}Na_xMnBi_2$, which reveals a vestigial linear frequency dependent behaviour of the optical conductivity in the mid-infrared, ascribed to electronic interband transitions involving Dirac bands. Furthermore, we uncover optical signatures for a partial gapping of the Fermi surface, for energy scales up to 0.2 eV, at the onset of the spin reorientation transition which also manifests as an anomaly in the *dc* transport data. This may reveal the inclination towards a Fermi surface instability in topological materials, possibly related to a density-wave order.

PACS numbers: 71.20.Gj,78.20.-e

Novel quantum phenomena emerge from the peculiar electronic properties of topological materials and attract much attention both theoretically and experimentally[1]. Their electronic structure is broadly characterised by the presence of Dirac states with the hallmark of a linear dispersion at the Dirac nodes, unlike the commonly observed quadratic one in conventional metals. Other important types of (mostly elusive) elementary quasiparticles in topological materials are Majorana and Weyl fermions, which are highly sought after in several novel superconductors, graphene, pyrochlore iridates, quasicrystals and transition metal monopnictides[1–7].

The quasi-two-dimensional bismuth layer-like AMnBi$_2$ (A = alkaline as well as rare earth atom) lately advanced as an arena for the investigation of low-energy quasiparticle excitations in topological materials[1]. The A = Sr or Ca compositions have attracted special attention because anisotropic Dirac cones may be realised[2,8]. This latter property can be exploited for making new electronic devices with electrons propagating differently from one direction to the other. AMnBi$_2$ (A = Sr or Ca) also shares several similarities with the crystal structure of iron-based superconductors and are considered to be bad-metals with a long-range antiferromagnetic order at temperatures T_N ranging between 270 and 290 K. Moreover, the *dc* resistivity ($\rho(T)$) in CaMnBi$_2$ displays an additional anomaly at $T_s \sim 50$ K, the origin of which is highly debated but seems to coincide with the onset of a spin reorientation, as a consequence of spin canting or weak ferromagnetic order[2,4,9]. In a broad context, low-dimensional magnetism and its putative relationship to the electronic properties are a central topic in condensed matter and call for a thorough approach from different experimental perspectives and materials.

In addition to angle-resolved photoemission spectroscopy (ARPES), optical investigations of the complete excitation spectrum prove to be a powerful experimental tool to address the consequences and peculiarities of the electronic dispersion in topological materials, as amply shown in Refs. 10–18. A generic and widely established feature in their optical response is the linear energy dependence at selected spectral ranges of the real part of the optical conductivity, which underlines the linear dispersion of the Dirac cones[19,20] or is a fingerprint of dispersive Dirac nodal lines[21].

Complementary to our previous work pointing out YbMnBi$_2$ as a Weyl semimetal and EuMnBi$_2$ as its more conventional semimetal counterpart[16], we provide here a thorough optical investigation of $Ca_{1-x}Na_xMnBi_2$ (x = 0, 0.03 and 0.05). We reveal the electronic interband transitions involving states associated with the Dirac cones. Another aim of this work is to address the impact on the electronic properties of the transition in $\rho(T)$ at T_s. At $T < T_s$, we discover a depletion of spectral weight in the optical conductivity at mid-infrared (MIR) energies, which seems to affect the electronic structure at the Dirac cones and also correlates with the extent of the anomaly in the *dc* transport properties. This may advance the proneness of topological materials towards a gapping of their Fermi surface (FS), as consequence of a density-wave order.

Our Na-doped CaMnBi$_2$ high quality single and well-characterised crystals were grown from high-temperature bismuth flux after the procedure described in Ref. 4. Prior data collections in high-vacuum cryostats, we freshly cleaved our specimens, thus achieving shiny surfaces of approximate size 2x2 mm^2. Electrical contacts for the $\rho(T)$ measurements were made using the silver paste to attach the Pt wires in a standard four-probe configuration[4]. We measure the T dependence of the optical reflectivity $R(\omega)$ at nearly normal incidence[22] with a Fourier-transform interferometer (Bruker Vertex 80v), working in the spectral range from the far-infrared (FIR) up to the near-infrared (NIR), i.e. between 30 and

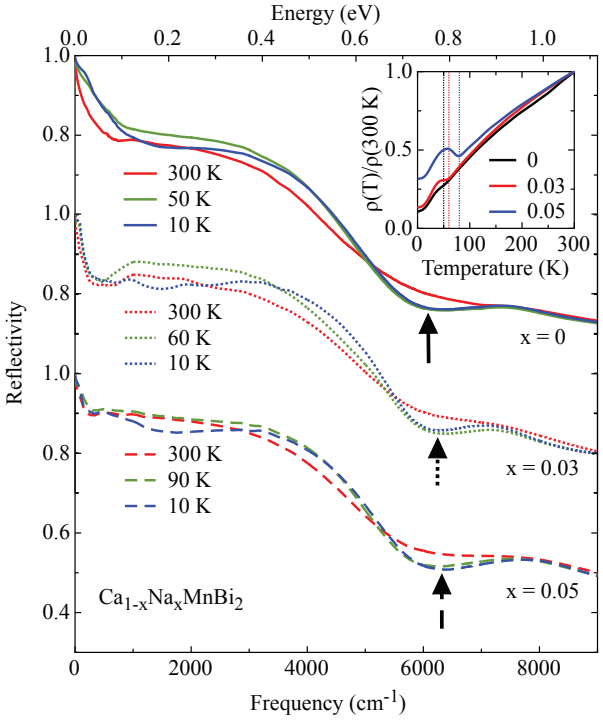

FIG. 1: (color online) Optical reflectivity $R(\omega)$ of selected $Ca_{1-x}Na_xMnBi_2$ compositions at 300 K, T_s and 10 K, emphasising its T dependence in the MIR range and highlighting the $R(\omega)$ plasma edge (vertical arrows at the plasma edge onset). The $R(\omega)$ curves for each doping are shifted vertically for clarity, and their axis covers the same interval everywhere. The inset shows $\rho(T)$ normalised at 300 K for the measured compositions. The thin dotted lines mark T_s (see text).

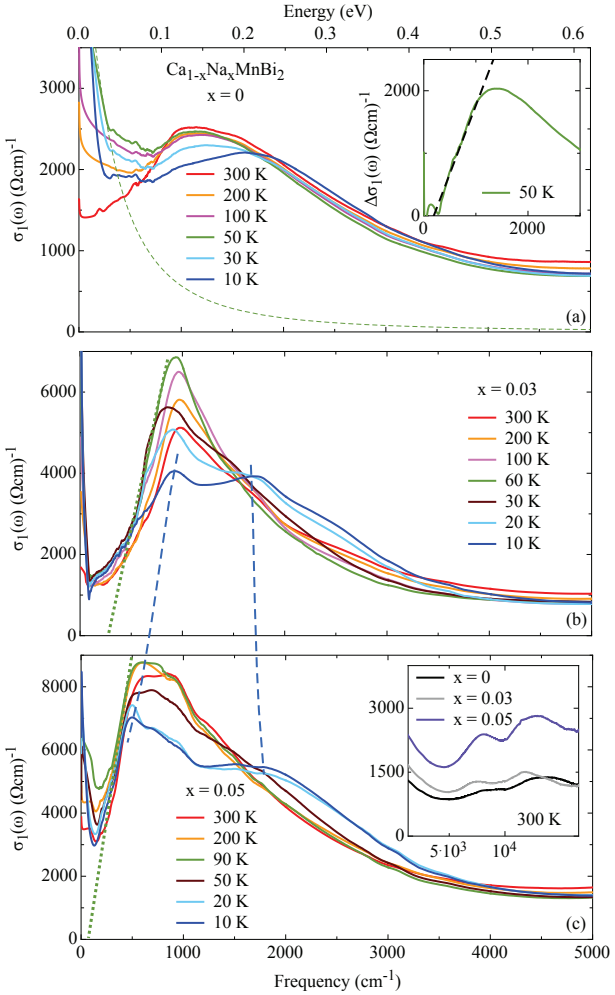

FIG. 2: (color online) Temperature dependence of the real part $\sigma_1(\omega)$ of the optical conductivity of $Ca_{1-x}Na_xMnBi_2$, highlighting the excitation spectrum at FIR and MIR frequencies. The inset in panel (a) displays $\Delta\sigma_1(\omega)$ at T_s, which underscores the $\sigma_1(\omega) \sim \omega$ behaviour after removing its metallic intraband contribution (thin dashed line in the main panel for $x = 0$), obtained by adding two Drude terms. The $\sigma_1(\omega) \sim \omega$ trend is emphasised in panels (b) and (c) for data at T_s (dotted lines), as well. The inset in panel (c) displays $\sigma_1(\omega)$ at 300 K for all investigated Na doping above 3000 and up to $2.5x10^4$ cm^{-1}. The blue dashed lines across the (b) and (c) panels emphasise the split into two peaks of the MIR absorption at 10 K (i.e, $< T_s$) upon increasing x.

12000 cm^{-1}. This set of data is complemented at room temperature with those obtained by the PerkinElmer Lambda 950 from NIR up to the ultra-violet (UV) range, i.e. 4000-48000 cm^{-1}. This is the prerequisite for reliable Kramers-Kronig transformation, giving access to the optical conductivity. To this end, standard and well-established extrapolation procedures of $R(\omega)$ are applied at low as well as high frequencies. In the *dc* limit (i.e., $\omega \to 0$) we use the Hagen-Rubens (HR) extrapolation of $R(\omega)$ ($R(\omega) = 1 - 2\sqrt{\frac{\omega}{\sigma_{dc}}}$) with *dc* conductivity (σ_{dc}) in agreement with the transport values[4]. Above the upper-frequency limit, we consider the extrapolation $R(\omega) \sim \omega^{-s}$ (with $s = 2$ up to twice the measured spectral range and $s = 4$ above, in order to simulate the electronic continuum)[22].

The inset in Fig. 1 displays the T dependence of $\rho(T)$ for all investigated Na doping, which is in broad agreement for $x = 0$ with previous data[4]. We remark the slightly concave T dependence of $\rho(T)$ prior to its bump-like anomaly with onset at $T_s \sim 50$ K ($x = 0$), ~ 60 K ($x = 0.03$) and ~ 90 K ($x = 0.05$), which gets stronger upon increasing the Na content. While not invariably detected, as in some transport investigations and Raman study of the title pristine compound[23,24], and totally absent in $\rho(T)$ of $SrMnBi_2$ below 300 K[25], there are by now several reports, establishing this anomaly in $\rho(T)$ as a robust experimental fact in $Ca_{1-x}Na_xMnBi_2$[4,9,26]. Its most natural implication is a partial gapping of FS. By assuming that the T dependence of the scattering rate is not altered by the transition at T_s as well as that the effective mass remains constant, we can already anticipate[27] that the $\rho(T)$-anomaly at its peak foresees a FS gapping of 12% ($x = 0$), 26% ($x = 0.03$) and 23% (x =0.05) (horizontal thick grey dashed line in Fig. 3), upon which we will return later.

The main panel of Fig. 1 reviews the metallic-like $R(\omega)$ of the investigated $Ca_{1-x}Na_xMnBi_2$ at 300 K, T_s and 10 K. The T dependence of $R(\omega)$ mainly develops at MIR frequencies for all compositions. $R(\omega)$ displays indeed a plasma edge at about 6000 cm^{-1} (black arrows in Fig. 1), which gets sharper at low T, and a rather broad MIR shoulder, prior approaching total reflection for $\omega \to 0$ in the FIR range. At MIR frequencies, $R(\omega)$ gets overall enhanced upon lowering T and then shows a depletion at frequencies varying between 1000 and 4000 cm^{-1} for $T < T_s$. Before going any further, it is worth pointing out that the $R(\omega)$ spectra of $Ca_{1-x}Na_xMnBi_2$ share some common features with recent data on $SrMnBi_2$[28], at least at high MIR frequencies. Nonetheless, $R(\omega)$ of $SrMnBi_2$ displays a depletion at $\omega < 2000$ cm^{-1}, which arises already below 300 K and is accompanied by the progressive development of a sharp plasma edge with onset at 1000 cm^{-1} upon lowering T. Such a behaviour was accounted for within a multiband electronic structure, so that the T dependence of the optical response is due to quasiparticles thermally redistributed into two conduction bands, therefore neglecting Dirac physics[28].

In Fig. 2, we compare the real part $\sigma_1(\omega)$ of the optical conductivity below 5000 cm^{-1} for all compositions as a function of T. We appreciate two features, upon which we will focus our attention for the rest of the paper. First, the zero-energy mode gets narrower with decreasing T and states explicitly the metallic contribution to the excitation spectrum[22]. The second feature is the MIR peak, displaying a remarkable T dependence. At $T > T_s$, this MIR absorption strengthens with increasing doping and even remarkably sharpens with decreasing T for $x = 0.03$. Upon lowering T, it shifts to higher energies with a broad low frequency tail for $x = 0$ and clearly splits into two distinct peaks at $T < T_s$ for the Na-doped compositions. The low frequency edge of the MIR absorption moves towards lower frequencies and displays a more pronounced linear behaviour (i.e., $\sigma_1(\omega) \sim \omega$) upon Na doping[29], yet always with a finite intercept with the frequency axis (dotted lines for data at T_s in Figs. 2(b) and (c)). We note that the optical response of $CaMnBi_2$ share similar absorption features with the structurally similar Weyl semimetal $YbMnBi_2$ and its gapped semimetal counterpart $EuMnBi_2$[16,17].

With the support of the electronic band structure calculations and its confirmation by ARPES[8,30], as well as driven by the characteristic $\sigma_1(\omega) \sim \omega$ signature, we propose to identify the MIR absorption with the interband transitions involving the Dirac bands located along the $\Gamma - M$ line of the Brillouin zone (BZ). It is intriguing that its linear frequency dependence in $\sigma_1(\omega)$ does not head to the origin, for all $T > T_s$ and x, as it would be expected for Dirac fermions[19]. Such a linear extrapolation at finite frequencies signals the gapping of the original massless Dirac cones. In fact, the presence of spin-orbit coupling (SOC) first moves the Fermi level into the lower Dirac cone and simultaneously splits the related bands so that a gap of about 50 meV (for $x = 0$) opens at the Dirac points[8,30]. The obvious shift to lower energies of the leading MIR edge upon Na doping for $T > T_s$ (Figs. 2(b) and (c)) may suggest that Na doping leads to a decrease of the necessary excitation energy for transitions across the gapped Dirac cones[20]. This could originate from the suppression of SOC because of the smaller mass of Na with respect to Ca. The T dependence of the MIR absorption for $T > T_s$ mainly reflect the effect due to Pauli blocking (i.e., forbidden optical transitions when the final states are filled). Reducing the thermal broadening with decreasing T induces a sharpening of the MIR optical excitation (Fig. 1 and specifically 2(b)).

Several other electronic interband transitions, from states located deep into the electronic structure (i.e., away from the Fermi level), certainly merge into the joint-density of states, as measured by $\sigma_1(\omega)$, and therefore are supposed to affect the absorption spectrum beyond the MIR energy interval. In fact, additional absorptions are observed in $\sigma_1(\omega)$ at the near-infrared (NIR) frequencies between 6000 and 15000 cm^{-1} (inset Fig. 2(c)) and are common to all doping.

It is a common procedure to extract an estimate for the Fermi velocity (v_F) from the slope of $\sigma_1(\omega) \sim \omega$[10–17]. Here, we limit our attention to $x = 0$, for which a comparison with the literature is feasible. We first subtract the metallic contribution to $\sigma_1(\omega)$ (dashed line in Fig. 2(a)), by modelling it within a multi-Drude approach[22]. This results in the quantity $\Delta\sigma_1(\omega)$, shown in the inset of Fig. 2(a), from where we achieve a value of $v_F \sim 2.1\text{x}10^4$ m/s at T_s[31], which agrees fairly well with the ARPES results[8], keeping in mind that optics averages over the whole reciprocal space[16]. A comprehensive phenomenological analysis with the aim to determine v_F for all Na doping is left for a future publication.

We now elaborate on the anomaly in $\rho(T)$ (inset Fig. 1) and its impact on $\sigma_1(\omega)$ and thus on the electronic properties. In this context, it is of interest to elucidate, how the spectral weight (SW) redistributes in the excitation spectrum as a function of T. The so-called integrated SW of the measured $\sigma_1(\omega)$ up to well-defined cut-off energies (ω_c) is given by:

$$SW(\omega_c; T) = \frac{120}{\pi} \int_0^{\omega_c} \sigma_1(\omega; T) d\omega \qquad (1)$$

This model-independent quantity is related to the number of the effective carriers (normalized by their effective mass) contributing to the optical processes up to ω_c. Therefore, in the $\omega_c \to \infty$ limit, it is expected to merge to a constant value at all T, satisfying the f-sum rule[22]. The full recovery of SW on our data is achieved at energies of about 1 eV (insets Fig. 3). For the purpose of our discussion, we will consider the ratio $SW(\omega_c; T)/SW(\omega_c; T_s)$ which emphasises the relevant energy scale of SW transfer at $T < T_s$. If there is a transfer of SW from high to low energies, the SW ratio will exceed 1 at low energies and then smoothly approach 1 upon increasing ω_c until the full energy scale of the low-energy resonance is

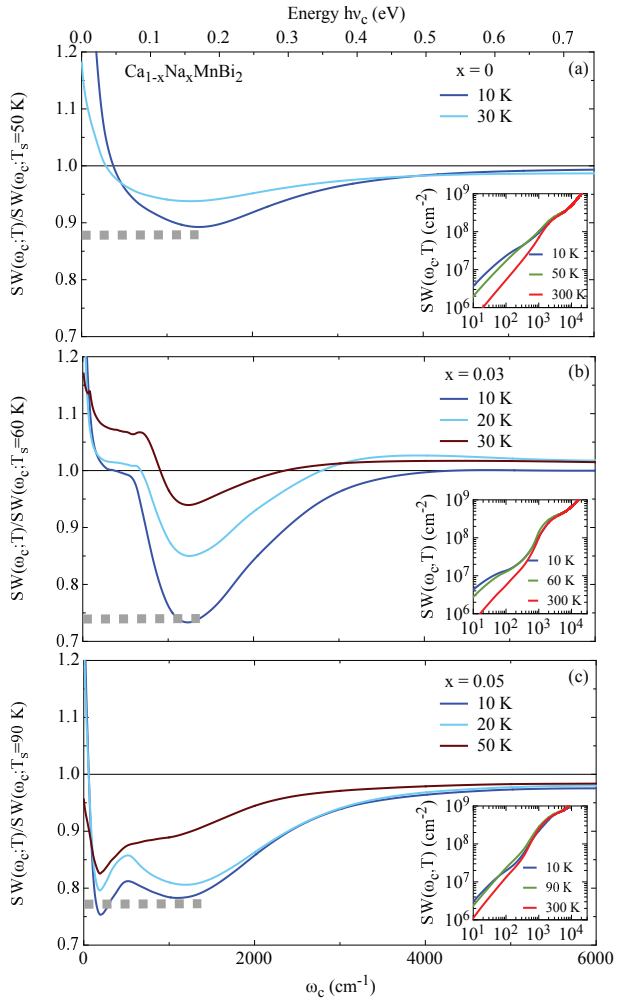

FIG. 3: (color online) The integrated spectral weight (SW) after Eq. 1, normalised by the same quantity at T_s, is shown at $T < T_s$ and as a function of the cut-off frequency ω_c. The insets show $SW(\omega_c; T)$ at 300 K, T_s and 10 K. The horizontal thick grey dashed line in each panel represents the estimated FS gapping from the $\rho(T)$ data (see text)[27].

reached. For instance, SW may move into the low energy metallic (Drude) mode. If there is a transfer of SW from low to high energies though (as it would occur by the opening of a gap), the SW ratio will fall below 1 until the total energy scale of SW transfer is reached. The SW ratio will then display a depletion, so that its minimum corresponds to the energy scale of the single-particle (partial) gap excitation within the electronic structure[22].

Figure 3 displays $SW(\omega_c; T)/SW(\omega_c; T_s)$ at selected $T < T_s$ and as a function of ω_c. The resulting redistribution of SW in $\sigma_1(\omega)$ mainly occurs from the FIR range up to the onset of the MIR peak and its high frequency tail. A substantial removal of SW from low to high energies of the order of 0.2 eV is indeed observed at $T < T_s$ for increasing Na doping. Therefore, in parallel to the enhancement of the anomaly in $\rho(T)$ upon Na doping (inset Fig. 1), a partial gapping of FS clearly emerges from the excitation spectra, as well. The SW reshuffling across T_s amounts to about 10 to 25% (i.e., the resulting depletion of the SW ratio) from $x = 0$ to 0.05, which agrees with the estimation of the FS gapping from the bump-like anomaly in $\rho(T)$ (horizontal thick grey dashed line in Fig. 3), as pointed out above. As it will be elaborated elsewhere, the reshuffling of SW across T_s and for all x (Fig. 3) agrees with the partial removal of the Drude weight towards high energy excitations, within the phenomenological Lorentz-Drude fit of $\sigma_1(\omega)$.

The observed splitting of the MIR feature particularly resolved for Na-doped $CaMnBi_2$ at $T < T_s$ (Figs. 2(b) and (c)) might then be the signature of gapped excitations because of an incipient folding of the BZ complemented by additional lifting of the degeneracy at the Dirac cones upon symmetry breaking due to some kind of spin- or charge-density-wave order (SDW or CDW, respectively), like in iron-pnictides[32,33], or spin-canting itself[17]. In general, the conventional Peierls instability driven by the FS nesting, typical for quasi-one-dimensional materials[34], or the momentum dependence of the electron-phonon coupling matrix elements, as lately advanced for 2H-$NbSe_2$[35,36], may lead to a CDW order. The formation of such an order in a Dirac fermion system, though, was recently addressed within the natural mechanism of electron-phonon coupling in layered-like honeycomb lattice[37,38], paving the way for realistic description of broken symmetry states in topological materials.

There is also an obvious accumulation of SW into the FIR frequency range of $\sigma_1(\omega)$ upon lowering T below T_s (Fig. 3), associated with the un-gapped portion of FS (Fig. 2). Its narrowing with decreasing T agrees with the overall metallic trend of $\rho(T)$ (inset Fig. 1) and particularly for $T < T_s$ is a signature of the switching-off of scattering channels in connection with the proposed FS gapping.

The putative FS gapping with apparent impact at the Dirac cones may also lead to a new interpretation of the similar MIR absorption seen in $SrMnBi_2$ at $T < 300$ K[28]. One might speculate that, instead of a mechanism based on the thermally-assisted indirect transitions within a multiband electronic structure[28], a FS instability with onset already above 300 K occurs in the latter compound. Consequently, chasing the related anomaly in $\rho(T)$ at $T > 300$ K may clarify this issue and confirm this scenario.

Finally, it is worth commenting, that a peak in $\rho(T)$ could also be caused by a T-driven topological quantum phase transition (TPT), involving an inversion of the valence and conduction bands[39]. However, the optical response in our Na-doped $CaMnBi_2$ shares little similarities with the expected signatures for TPT, as recently shown in the case of the intermediate Dirac semimetal $ZrTe_5$[40].

In conclusion, we reveal the optical fingerprints of the electronic properties in the Dirac material $Ca_{1-x}Na_xMnBi_2$. We provide optical evidence for an incipient FS gapping at $T < T_s$, which turns out to pair

with the anomaly in $\rho(T)$ at T_s and to strengthen with Na doping. We conjecture that the spin-reorientation occurring below T_s could be driven by a density-wave order directly affecting the electronic structure at the Dirac cones. Our findings may generally underline the proneness towards FS instabilities in topological materials.

Acknowledgements

This work was partially supported by the Swiss National Science Foundation (SNSF). Work at Brookhaven National Laboratories was supported by the U.S. DOE-BES, Division of Materials Science and Engineering, under Contract No. DE-SC0012704.

[+] Both authors equally contributed to the experimental work.

[†] Present address: School of Physics, Chongqing University, Chongqing 400044, China

[*] Correspondence and requests for materials should be addressed to: L. Degiorgi, Laboratorium für Festkörperphysik, ETH - Zürich, 8093 Zürich, Switzerland; email: degiorgi@solid.phys.ethz.ch

[1] M. Z. Hasan and C. L. Kane, Rev. Mod. Phys. **82**, 3045 (2010) and references therein.
[2] J. Park, G. Lee, F. Wolff-Fabris, Y. Y. Koh, M. J. Eom, Y. K. Kim, M. A. Farhan, Y. J. Jo, C. Kim, J. H. Shim, and J. S. Kim, Phys. Rev. Lett. **107**, 126402 (2011).
[3] K. Wang, D. Graf, H. Lei, S. W. Tozer, and C. Petrovic, Phys. Rev. B **84**, 220401(R) (2011).
[4] K. Wang, D. Graf, L. Wang, H. Lei, S. W. Tozer, and C. Petrovic, Phys. Rev. B **85**, 041101(R) (2012).
[5] A. F. May, M. A. McGuire, and B. C. Sales, Phys. Rev. B **90**, 075109 (2014).
[6] P. Richard, K. Nakayama, T. Sato, M. Neupane, Y.-M. Xu, J. H. Bowen, G. F. Chen, J. L. Luo, N. L. Wang, X. Dai, Z. Fang, H. Ding, and T. Takahashi, Phys. Rev. Lett. **104**, 137001 (2010).
[7] K. S. Novoselov, A. K. Geim, S. V. Morozov, D. Jiang, M. I. Katsnelson, I. V. Grigorieva, S. V. Dubonos, and A. A. Firsov, Nature **438**, 197 (2005).
[8] Y. Feng, Z. Wang, C. Chen, Y. Shi, Z. Xie, H. Yi, A. Liang, S. He, J. He, Y. Peng, X. Liu, Y. Liu, L. Zhao, G. Liu, X. Dong, J. Zhang, C. Chen, Z. Xu, X. Dai, Z. Fang, and X. J. Zhou, Scientific reports **4**, 5385 (2014).
[9] J. B. He, D. M. Wang, and G. F. Chen, Appl. Phys. Lett. **100**, 112405 (2012).
[10] R. Y. Chen, S. J. Zhang, J. A. Schneeloch, C. Zhang, Q. Li, G. D. Gu, and N. L. Wang, Phys. Rev. B **92**, 075107 (2015).
[11] A. B. Sushkov, J. B. Hofmann, G. S. Jenkins, J. Ishikawa, S. Nakatsuji, S. Das Sarma, and H. D. Drew, Phys. Rev. B **92**, 241108(R) (2015).
[12] T. Timusk, J. P. Carbotte, C. C. Homes, D. N. Basov, and S. G. Sharapov, Phys. Rev. B **87**, 235121 (2013).
[13] B. Xu, Y. M. Dai, L. X. Zhao, K. Wang, R. Yang, W. Zhang, J. Y. Liu, H. Xiao, G. F. Chen, A. J. Taylor, D. A. Yarotski, R. P. Prasankumar, and X. G. Qiu, Phys. Rev. B **93**, 121110(R) (2016).
[14] D. Neubauer, J. P. Carbotte, A. A. Nateprov, A. Löhle, M. Dressel, and A. V. Pronin, Phys. Rev. B **93**, 121202(R) (2016).
[15] A. Akrap, M. Hakl, S. Tchoumakov, I. Crassee, J. Kuba, M. O. Goerbig, C. C. Homes, O. Caha, J. Novák, F. Teppe, W. Desrat, S. Koohpayeh, L. Wu, N. P. Armitage, A. Nateprov, E. Arushanov, Q. D. Gibson, R. J. Cava, D. van der Marel, B. A. Piot, C. Faugeras, G. Martinez, M. Potemski, and M. Orlita, Phys. Rev. Lett. **117**, 136401 (2016).
[16] M. Chinotti, A. Pal, W. J. Ren, C. Petrovic, and L. Degiorgi, Phys. Rev. B **94**, 245101 (2016).
[17] D. Chaudhuri, B. Cheng, A. Yaresko, Q. D. Gibson, R. J. Cava, and N. P. Armitage, Phys. Rev. B **96**, 075151 (2017).
[18] Y. Shao, Z. Sun, Y. Wang, C. Xu, R. Sankar, A. J. Breindel, C. Cao, M. M. Fogler, A. J. Millis, F. Chou, Z. Li, T. Timusk, M. B. Maple, and D. N. Basov, PNAS **116**, 1168 (2019).
[19] C. J. Tabert and J. P. Carbotte, Phys. Rev. B **93**, 085442 (2016).
[20] S. P. Mukherjee and J. P. Carbotte, J. Phys.: Condens. Matter **29**, 425301 (2017).
[21] S. Ahn, E.J. Mele, and H. Min, Phys. Rev. Lett. **119**, 147402 (2017).
[22] M. Dressel and G. Grüner, *Electrodynamics of Solids*, Cambridge University Press, Cambridge, England (2002).
[23] A. Zhang, C. Liu, C. Yi, G. Zhao, T.-l. Xia, J. Ji, Y. Shi, R. Yu, X. Wang, C. Chen, and Q. Zhang, Nature Communications **7**, 13833 (2016).
[24] Y. F. Guo, A. J. Princep, X. Zhang, P. Manuel, D. Khalyavin, I. I. Mazin, Y. G. Shi, and A. T. Boothroyd, Phys. Rev. B **90**, 075120 (2014).
[25] Y. J. Jo, J. Park, G. Lee, M. J. Eom, E. S. Choi, J. H. Shim, W. Kang, and J. S. Kim, Phys. Rev. Lett. **113**, 156602 (2014).
[26] A. Wang, D. Graf, L. Wu, K. Wang, E. Bozin, Y. Zhu, and C. Petrovic, Phys. Rev. B **94**, 125118 (2016).
[27] The estimation of the FS gapping from $\rho(T)$ is calculated with the formula $[(\sigma_{norm} - \sigma_{peak})/\sigma_{norm}]$, where σ_{peak} is the *dc* conductivity at its anomaly minimum at T_{peak} and σ_{norm} is its expected 'normal' value without anomaly at the same T_{peak}, simply obtained from a linear interpolation of $\sigma(T) \sim 1/\rho(T)$ (inset Fig. 1) between 10 K and T_s (N.P. Ong and P. Monceau, Phys. Rev. B **16**, 3443 (1977)).
[28] H. J. Park, B. C. Park, M.-C. Lee, D. W. Jeong, J. Park, J. S. Kim, H. S. Ji, J. H. Shim, K. W. Kim, S. J. Moon, H.-D. Kim, D.-Y. Cho, and T. W. Noh, Phys. Rev. B **96**, 155139 (2017).
[29] While the $\sigma_1(\omega) \sim \omega$ behaviour is particularly evident for Na-doped compositions, it can be identified for $x = 0$, as well. This is explained later in relation to the estimation

of the Fermi velocity (see caption of Fig. 2).

[30] G. Lee, M. A. Farhan, J. S. Kim, and J. H. Shim, Phys. Rev. B **87**, 245104 (2013).

[31] v_F is derived from the formula $v_F \simeq \frac{NG_0}{24}(\frac{\Delta\sigma_1}{\Delta\omega})^{-1}$, G_0 being the quantum conductance, N the number of Dirac points and $\frac{\Delta\sigma_1}{\Delta\omega}$ the slope of the linear behaviour in $\sigma_1(\omega)$ (Fig. 2), calculated at finite energy intervals (P. Hosur, S. A. Parameswaran, and A. Vishwanath, Phys. Rev. Lett. **108**, 046602 (2012) and Ref. 16). For $CaMnBi_2$, $N = 8$.

[32] W. Z. Hu, J. Dong, G. Li, Z. Li, P. Zheng, G. F. Chen, J. L. Luo, and N. L. Wang, Phys. Rev. Lett. **101**, 257005 (2008).

[33] F. Pfuner, J. G. Analytis, J.-H. Chu, I. R. Fisher, and L. Degiorgi, Eur. Phys. J. B **67**, 513 (2009).

[34] G. Grüner, *Density Waves in Solids*, Addison-Wesley, Reading (1994), and references therein.

[35] X. Zhu, Y. Cao, J. Zhang, E. W. Plummer, and J. Guo, PNAS **112**, 2367 (2015).

[36] F. Zheng and J. Feng, Phys. Rev. B **99**, 161119(R) (2019).

[37] C. Chen, X. Y. Xu, Z. Y. Meng, and M. Hohenadler, Phys. Rev. Lett. **122**, 077601 (2019).

[38] Y.-X. Zhang, W.-T. Chiu, N. C. Costa, G. G. Batrouni, and R. T. Scalettar, Phys. Rev. Lett. **122**, 077602 (2019).

[39] G. Manzoni, L. Gragnaniello, G. Autès, T. Kuhn, A. Sterzi, F. Cilento, M. Zacchigna, V. Enenkel, I. Vobornik, L. Barba, F. Bisti, P. Bugnon, A. Magrez, V. N. Strocov, H. Berger, O. V. Yazyev, M. Fonin, F. Parmigiani, and A. Crepaldi, Phys. Rev. Lett. **117**, 237601 (2016).

[40] B. Xu, L. X. Zhao, P. Marsik, E. Sheveleva, F. Lyzwa, Y. M. Dai, G. F. Chen, X. G. Qiu, and C. Bernhard, Phys. Rev. Lett. **121**, 187401 (2018).